Applied Physics Express

LETTER • **OPEN ACCESS**

Development of laser-combined scanning multiprobe spectroscopy and application to analysis of $WSe_2/MoSe_2$ in-plane heterostructure

To cite this article: Hiroyuki Mogi *et al* 2019 *Appl. Phys. Express* **12** 045002

OPEN ACCESS

Applied Physics Express 12, 045002 (2019) LETTER

https://doi.org/10.7567/1882-0786/ab09b9

Development of laser-combined scanning multiprobe spectroscopy and application to analysis of $WSe_2/MoSe_2$ in-plane heterostructure

Hiroyuki Mogi[1†], Zi-Han Wang[1†], Takafumi Bamba[1], Yuhei Takaguchi[2], Takahiko Endo[2], Shoji Yoshida[1], Atsushi Taninaka[1], Haruhiro Oigawa[1], Yasumitsu Miyata[2], Osamu Takeuchi[1], and Hidemi Shigekawa[1*]

[1]*Faculty of Pure and Applied Sciences, University of Tsukuba, Tsukuba, 305-8573, Japan*
[2]*Department of Physics, Tokyo Metropolitan University, Tokyo 192-0397, Japan*

[*]E-mail: hidemi@ims.tsukuba.ac.jp
[†]These two authors contributed equally to this work.

Received February 6, 2019; accepted February 22, 2019; published online March 13, 2019

By combining scanning multiprobe (MP) microscopy with optical methods such as light-modulated spectroscopy (LMS) and optical pump-probe (OPP) method, we have succeeded in developing a microscopy method for measuring electronic structures and photoinduced carrier dynamics in microscopic structures. We demonstrated its performance by analyzing the electronic structures in a monolayer island of a $WSe_2/MoSe_2$ in-plane heterostructure grown on a SiO_2/Si substrate. By observing the field-effect transistor characteristics and photocurrent mapping over the heterostructure by LMS, we were able to visualize the band structure. Positional dependence of carrier dynamics was also successfully probed by OPP-MP spectroscopy. © 2019 The Japan Society of Applied Physics

In current material science and its applications to the development of device technologies, the use of the low-dimensional functions realized in materials such as topological insulators[1)] and mono-to-multilayer transition metal dichalcogenides (TMDCs)[2)] has been attracting considerable attention. To advance such study, the in-depth understanding and control of local electronic structures and their dynamics in microscopic structures are essential.[3)] For such purposes, for example, scanning tunneling microscopy (STM) has been used to evaluate the band structure,[4–6)] and by forming metal electrodes using techniques such as lithography, time-resolved photocurrent measurement[7)] which is an application of the optical pump-probe (OPP) method[8)] has been used to observe ultrafast carrier dynamics. In the case of small device structures such as a microscopic TMDC island formed on a insulative material, wired electrodes can be prepared to enable conductive measurement, which, however, requires physical and chemical treatments of samples.[9)] A possible approach is to apply multiprobe (MP) STM techniques, in which multiple tips are used to measure, for example, transport characteristics between two desired points.[10)]

To obtain information on photoinduced phenomena, optical technologies must be introduced into the MP techniques. We have been developing laser-combined STM and related techniques, light-modulated scanning tunneling spectroscopy (LM-STS)[11)] and OPP-STM,[12,13)] and have been applying them in the field of nanoscale science.

In LM-STS, by simultaneously measuring the relationship between tunnel current I_t and bias voltage V (I–V curve measurement) while alternately turning the photoillumination on and off using a chopper, one can obtain and visualize information such as the local band structure,[11)] carrier transport in a p–n junction,[14)] photocarrier generation in a solar cell structure,[15)] and surface photovoltage (SPV) effect on a phase transition.[16)] In OPP-STM, on the other hand, femtosecond temporal resolution and STM spatial resolution were simultaneously realized in a microscopy by combining ultrashort pulse technology, such as OPP method, with STM. The sample below the STM tip was photoilluminated by a train of ultrashort laser pulse pairs (pump and probe pulses) with a certain delay time t_d, and the tunnel current measured as a function of the delay time $I_t(t_d)$ gives local information of the ultrafast carrier dynamics while simultaneously providing an STM image of the local structure.[13,17,18)] A nonequilibrium carrier distribution, for example, was generated with ultrashort laser pulses and its relaxation processes were probed using the STM tunneling current. Using OPP-STM, one can achieve for example, direct measurement of the hole-capture rate at a single impurity state in GaAs,[19)] and visualization of the ultrafast carrier dynamics in a pin structure.[20)]

LM-STS and OPP-STM are useful techniques; however, only one STM tip has been used to probe electronic structures and their dynamics immediately below the STM tip. Therefore, in the case of small structures such as TMDC island structures formed on an insulative material, measurement cannot be carried out because of the low conductivity of such structures, and multiple probes are necessary to form a circuit. For further advances to observe dynamics such as the transport of current and spin in small structures, MP microscopy that enables probing correlations of the dynamics between different locations at desired locations is a key requirement. However, the simultaneous use of MP techniques with laser technology has not been realized because of the difficulties that arise when the two advanced technologies are combined.

Here, we present a microscopy method that we have developed by combining MP techniques with optical methods such as LM-STS and OPP-STM. By observing the field-effect transistor (FET) characteristics and photocarriers in a monolayer island of a $WSe_2/MoSe_2$ in-plane heterostructure grown on a SiO_2 substrate, we were able to visualize the band structure. Positional dependent carrier dynamics was also successfully probed by OPP-MP spectroscopy.

Figure 1 shows a schematic illustration of our newly developed laser-combined MP system. Laser-combined STM and MP-STM are well-realized technologies as measurement methods, but there are some additional issues to be resolved

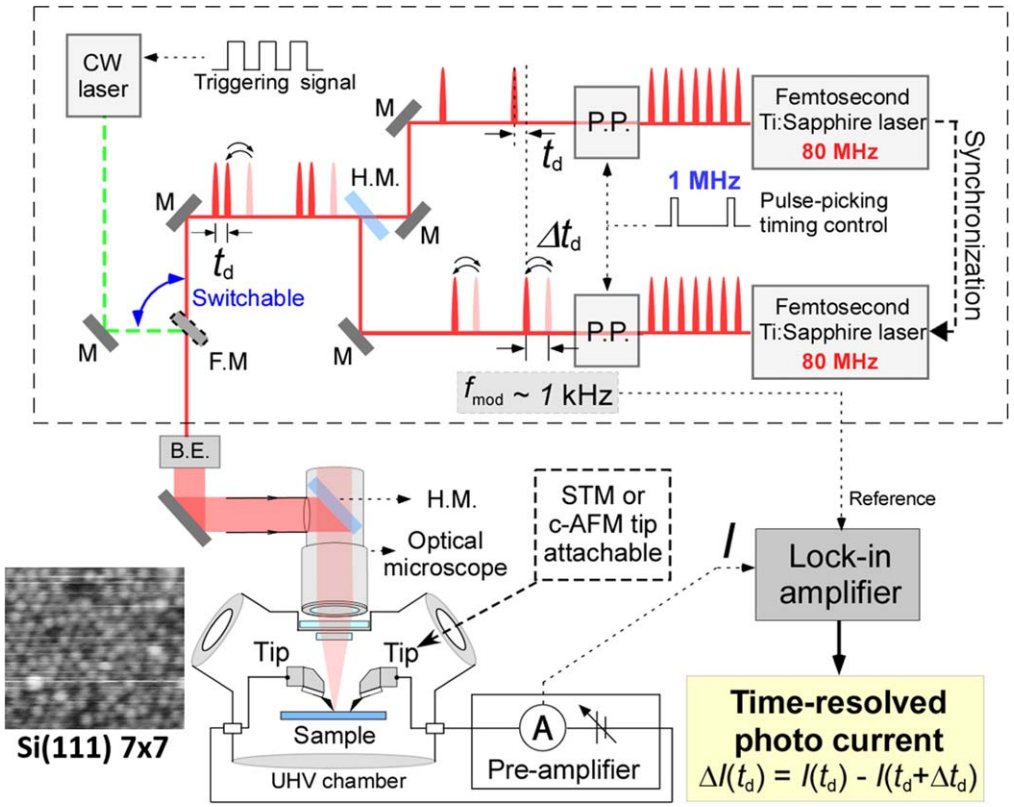

Fig. 1. (Color online) Schematic illustration of the developed MP spectroscopy system. The system consists of two synchronized lasers with a pulse width of ~150 fs, which can be changed to a continuous-wave laser with a chopper when experiments such as LM-STS are carried out. A high-resolution optical microscope (~1 μm spatial resolution) with an optical access port was attached outside the main UHV chamber of the MP system, which was oriented perpendicular to the sample plate. This particular design not only provides a way of checking the locations of the sample surface and tips but also has excellent laser focusability. The STM/ c-AFM tip was attached diagonally so that its apex could be more clearly seen from above. The delay time between the pump and probe pulses was modulated between t_d and $t_d + \Delta t_d$ at ~1 kHz for lock-in detection. M, mirror; H.M., half mirror; F.M., flip mirror; P.P., pulse picker; B.E., beam expander; I, current signal; Δt_d; difference between the two delay times used for modulation; V_s, sample bias voltage; f_{mod}, delay time modulation frequency. Conductive AFM(c-AFM) cantilevers coated with $PtIr_5$ (0.2 N m^{-1}) were used in this experiment. Contact was detected by the change in the capacitance between the Si gate and cantilever. Si(111)-7 × 7 image was taken to show the performance of this system. Since resistance of the target sample on this paper was more than GΩ, it was difficult to stably scan the STM tip to obtain an image with a good quality.

to combine them. Two typical examples are as follows: (1) in ordinary OPP-STM using one probe, light is irradiated to the tip of the probe through one of two windows on the side of the vacuum chamber at symmetrical positions with respect to the sample. In addition to the measurement of tunnel current, the reflected light is extracted through the other window for OPP measurement so that both results can be compared. However, when combined with a MP system, incident light may be blocked by the complicated shape of the probe heads. (2) Moreover, in this arrangement, it is necessary to confirm the irradiation light spot on the sample by placing the zoom lens at a position far from the sample (for example, at a distance of 180 mm, NA = 0.083). Therefore, it becomes more difficult to precisely control the light spot position. In addition, in an ordinary MP system, scanning electron microscopy (SEM) is used to evaluate samples and the positioning of probes. However, some samples are damaged by the high-energy electron beam irradiation during the observation, and the deposition of contaminants such as hydrocarbons may occur. Furthermore, when the stiff probes are mechanically brought into contact with the sample, the probes and the sample may be deformed.

To solve these problems, we combined a long-focus optical microscope system (working distance: 24 mm, NA = 0.42) for positioning the probe and light irradiation. Although the spatial resolution of an optical microscope (~1 μm) was inferior to that of a SEM, in addition to solving the above problems, it became possible to irradiate light from directly above the probe via a half mirror mounted inside the optical microscope and the spot size was reduced to ~1 μm.

The vibration noise of the probe head section was reduced by isolating the spring vibration using an eddy current damper. However, as the spot size became smaller, when the probe stage shook against the light beam, it directly led to the fluctuation of light intensity, and it was found that enhancement of the vibration isolation performance was necessary. Therefore, the number of magnets in the eddy current damper was increased, and the air spring isolation stage supporting the entire device was changed from a passive type to an active type to enhance the vibration isolation performance. As a result, the fluctuation of the probe stage at the spring suspension could be reduced to about 100 nm order. When mechanical contact was necessary, conductive atomic force microscopy (c-AFM) cantilevers were used instead of stiff STM probes to avoid the deformation of the probe tip and sample. We have developed a probe holder for the compatible use of an STM tip and a c-AFM cantilever, which also does not block the incident light. The STM tip was used to obtain atomic resolution when required in the experiment.

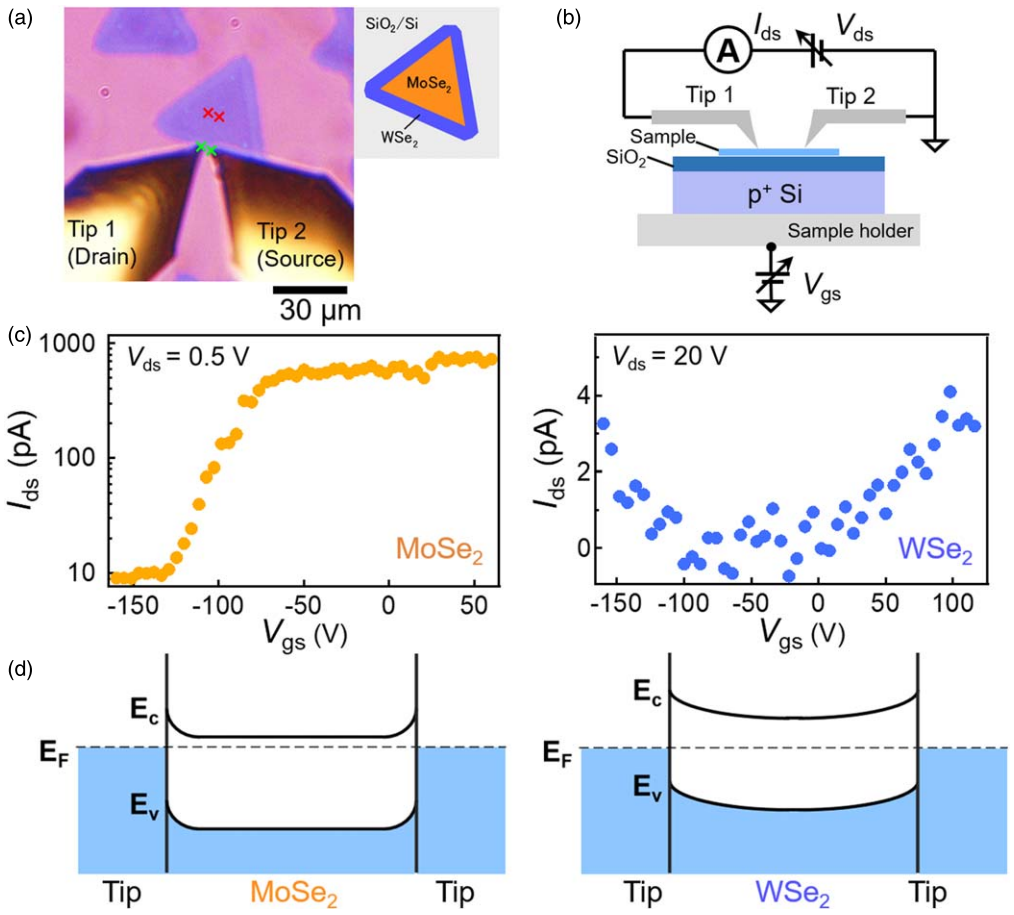

Fig. 2. (Color online) FET characteristic measurement. (a) Optical image of $WSe_2/MoSe_2$ in-plane heterostructure formed on SiO_2/Si substrate. (b) Schematic illustration of measurement setup. I_{ds}, drain–source current; V_{ds}, drain–source voltage; V_{gs}, gate–source voltage. (c) I_{ds} as a function of V_{gs} obtained for the V_{ds} kept at 0.5 V (left) and 20 V (right). (d) Band structures of WSe_2 and $MoSe_2$ estimated from the results shown in (c). E_v, energy of the valence band edge; E_c, Energy of the conduction band edge; E_F, Fermi energy. The figures illustrate the mutual relationship of band structures on relative scales (not actual values).

Next, to demonstrate the performance of the newly developed laser-combined MP system, three experiments, (1) analysis of the FET characteristics and photocarrier mapping, (2) light-modulated spectroscopy (LMS), and (3) time-resolved spectroscopy with an ultrashort pulse laser, were carried out to analyze the electronic structures in a monolayer island of a $WSe_2/MoSe_2$ in-plane heterostructure. Figure 2(a) shows an optical image of the sample. Isolated $WSe_2/MoSe_2$ islands grown on a SiO_2/Si substrate by halide-assisted chemical vapor deposition[21] were observed, in which a triangular $MoSe_2$ single layer was surrounded by a WSe_2 single layer. In some cases [e.g., upper right area of Fig. 2(a)], another shape was formed owing to different growth conditions.[22]

First, by observation of the FET characteristics and photocurrent mapping over the heterostructure by LMS, the band structure of the $WSe_2/MoSe_2$ in-plane heterostructure was analyzed. The FET characteristics were measured in the experimental setup shown in Fig. 2(b). Two c-AFM tips coated with $PtIr_5$ were placed in contact with the sample in the $MoSe_2$ or WSe_2 area to act as the source and drain. Then, while maintaining the voltage applied between the two tips V_{ds} at a certain value, the source–drain current between the two tips (I_{ds}) was measured as a function of the gate voltage V_{gs} applied between the Si substrate and the source tip.

Figure 2(c) shows the results obtained. A larger current was observed in the $MoSe_2$ region. In the $MoSe_2$ region, the current decreased when V_{gs} was negative, indicating that the $MoSe_2$ sample has n-type characteristics. On the other hand, in the WSe_2 region, the rise in current was similar at both positive and negative voltages, indicating the characteristics of an undoped sample. The slight shift with respect to origin suggests that the sample is slightly n-type. Although both materials were undoped, the $MoSe_2$ region, which grew first, was supposed to be more defective. In general, p-type characteristics are difficult to obtain for these materials,[23] and when Se atoms are desorbed, n-type characteristics are expected to be introduced.[24,25] Based on these results, Schottky barrier at $MoSe_2$ did not suppress the current compared with the barrier at the WSe_2, possible band structures for the $MoSe_2$ (band gap: 1.6 eV) and WSe_2 (band gap: 1.7 eV) regions[26] with $PtIr_5$ coated tips are shown in Fig. 2(d). The steepness of the band bending depends on the amount of doping (almost undoped in the WSe_2 region).

Next, to investigate the electronic structures of the $MoSe_2/WSe_2$ interface and the Schottky barriers formed between the tip and sample, LMS measurement was carried out. Figure 3(a) shows a schematic illustration of the measurement setup and the light spot used. Tips 1 and 2 were located in the $MoSe_2$ and WSe_2 regions, respectively. LMS measurement was carried out at the nine positions shown in Fig. 3(b) using continuous-wave light of 532 nm. While the value of V_g was maintained at +40 V, I_{ds} was

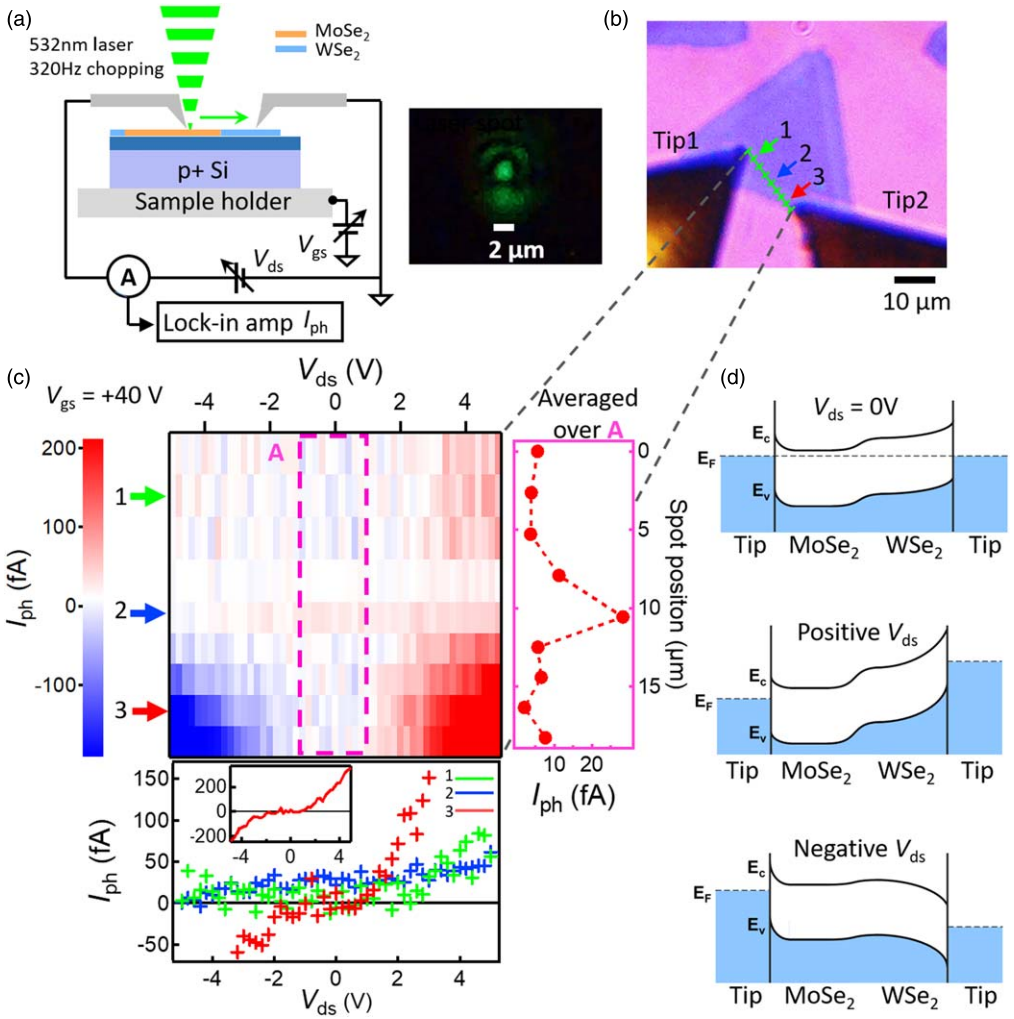

Fig. 3. (Color online) LMS measurement. (a) Schematic illustration of measurement setup and an optical image of the laser spot used. (b) Optical image of the two tips located on a $WSe_2/MoSe_2$ in-plane heterostructure island. (c) Results obtained by LMS along the green line shown in (b): I_{ph} (color scale) as a function of V_{ds} and the laser spot position shown in (b). Graph in the lower part indicates the cross sections along 1–3 which correspond to the positions shown in (b), where second positions from the edges were chosen for 1 and 3 to avoid the effect of shadow by tips. The inset shows a large scale feature of spectrum 1. Graph on the right side indicates the cross section averaged in the rectangular area A in the center color image. (d) Possible band structure of the $WSe_2/MoSe_2$ in-plane heterostructure estimated from the results shown in Figs. 2 and 3(c). The figures illustrate the mutual relationship of band structures on relative scales (not actual values).

measured as a function of V_{ds} by the lock-in detection method with the light intensity modulated at 320 Hz. The difference in the current ΔI_{ds} (=I_{ph}, photocurrent) between the conditions with and without illumination shows the effect of charge separation caused by the in-plane electric field including the built-in field at the interface and Schottky barrier.[27)]

Figure 3(c) shows the results obtained three-dimensionally. The positions indicated by the blue, green, and red arrows in Figs. 3(b) and 3(c) correspond to that of Tip 1, interface and Tip 2. The cross section in the lower part shows the I_{ph}–V_{ds} curves measured at the positions 1–3. The blue, green, and red lines correspond to the cross sections along the lines 1–3, indicated by arrows with the same color. The direction of I_{ph} reversed with the polarity of V_{ds} for the curve 3 (red line), indicating the similar change in the band bending caused by the Schottky barrier at the position 3 (Tip 2 position). The charge separation of excitons occurred in the depletion layer, and current was detected because (1) the Schottky barrier formed between Tip 1 and $MoSe_2$ did not interrupt the electron flow apparently [see Fig. 2(c)] for $V_{ds} \geqq 0$, and (2) the barrier at the hetero interface for holes was weakened for $V_{ds} < 0$, as shown in Fig. 3(d).

For the curves 1 and 2, I_{ph} was almost 0 in the negative bias region. I_{ph} similarly increased with the V_{ds} to +4 V, however, I_{ph} was slightly larger for the curve 2 around $V_{ds} = 0$, which is considered to be due to the existence of the built-in potential at the interface. To confirm this point, I_{ph} was averaged over the rectangular area A and shown in the cross section on the right side of Fig. 3(c). There is a clear peak around the interface, indicating the existence of the built-in potential.[9)] The increase in I_{ph} in the WSe_2 region compared to that in the $MoSe_2$ region also suggests the existence of the inner potential. Figure 3(d) shows possible band structures of the $WSe_2/MoSe_2$ in-plane heterostructure ($V_{ds} = 0$, positive, negative) visualized based on the results analyzed above.

Finally, we show the positional dependence of time-resolved measurement realized by the OPP-MP spectroscopy we have developed. The dynamics of photocarriers we have observed statically in the experiments above can be locally probed. Figure 4(a) shows the experimental setup. Four

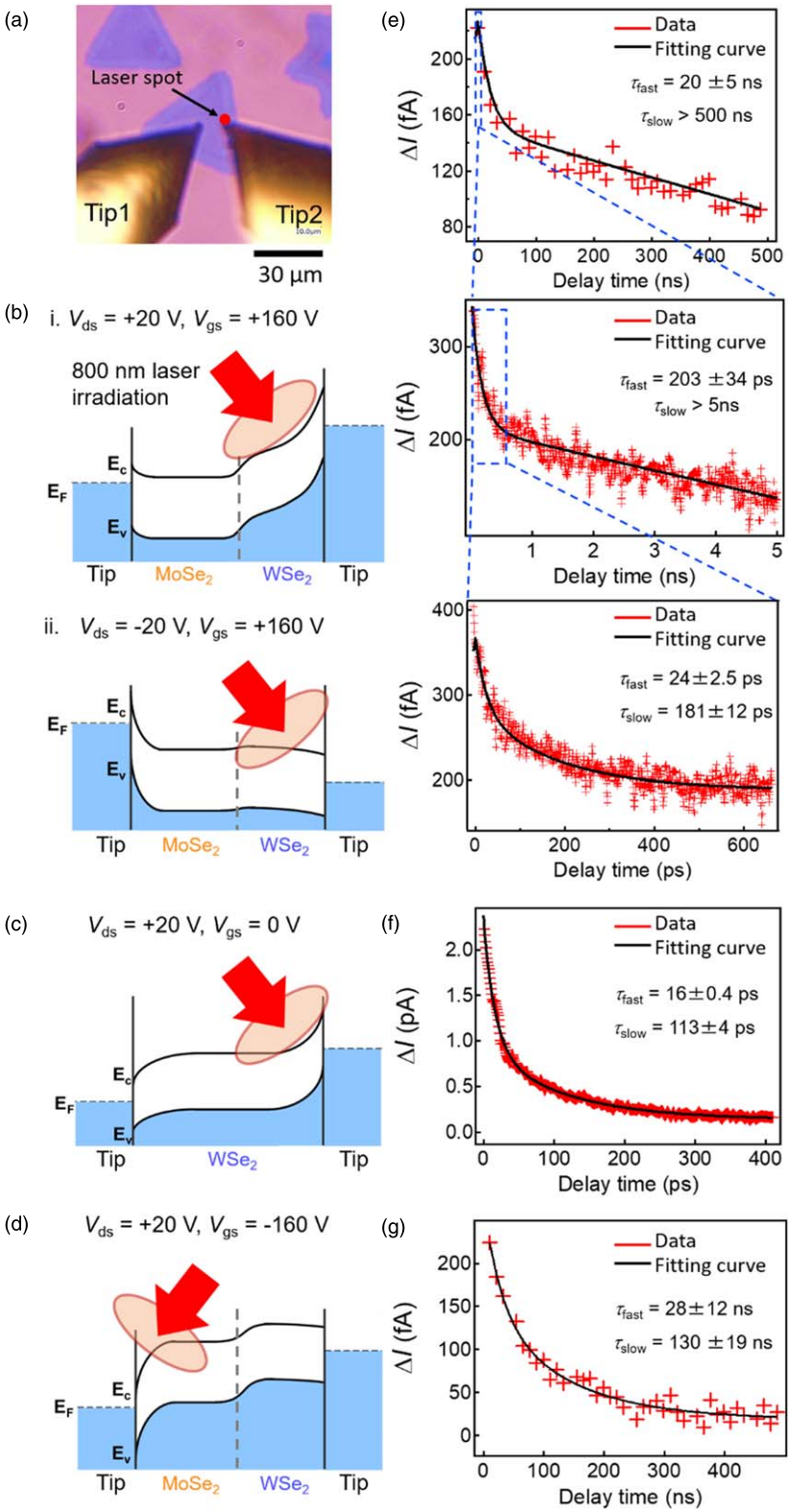

Fig. 4. (Color online) Results of OPP-MP spectroscopy. (a) Optical image of the experimental setup. (b)–(d) Schematic illustrations of the four experiments with different relations between the two tip positions, laser spot positions (at Tip 1 apex or Tip 2 apex), V_{ds}, and V_{gs}, with the conditions expressed as follows in the form (Tip 1 position, Tip 2 position, laser spot position, V_{ds}, V_{gs}): (b)-i (in $MoSe_2 \sim 10$ μm from interface, in $WSe_2 \sim 500$ nm from interface, at Tip 2 apex, +20 V, +160 V), (b)-ii (in $MoSe_2 \sim 10$ μm from interface, in $WSe_2 \sim 500$ nm from interface, at Tip 2 apex, −20 V, +160 V), (c) (in WSe_2, in WSe_2, at Tip 2 apex, +20 V, 0 V), (d) (in $MoSe_2 \sim 10$ μm from interface, in $WSe_2 \sim 500$ nm from interface, at Tip 1 apex, +20 V, −160 V). (e)–(g) Time-resolved spectra obtained for the experimental setups shown in (b)-i, (c), and (d). The spectra obtained in three different delay time ranges are shown in (e) to show details. Here, V_{gs} was adjusted to control the band bending at the laser spot position. The laser power was 16 mW, and the spot size was about 1.8 μm. The figures illustrate the mutual relationship of band structures on relative scales (not actual values).

experiments were carried out with different relations between the two tip positions, laser spot positions, V_{ds}, and V_{gs}, which are schematically shown in Figs. 4(b)–4(d). The figures illustrate the mutual relationship on relative scales of band structures between tips and sample under different experimental conditions.

A pulse train with an arbitrary repetition period was generated by the pulse picking method with a Pockels cell. It is possible to generate pulse pairs (pump and probe pulses) with a certain delay time by adjusting the synchronization system and the timing of pulse picking on each optical axis. When the sample surface is photoilluminated, the transient photocurrent is generated via charge separation due to the in-plane electric field. Then, when a probe pulse arrives during the relaxation processes such as recombination, change in photovoltage, and trapping,[19,28,29] an additional photocurrent is induced and changes the total magnitude of current depending on t_d,[20] providing time-resolves spectra. The photon energy of 1.55 eV (800 nm) was larger than the absorption edges of the excitons in the $MoSe_2$ and WSe_2 (~1.0 eV).[30]

First, experiments were carried out by placing Tip 1 and Tip 2 in the $MoSe_2$ and WSe_2 regions, respectively, as shown in Fig. 4(b). Figure 4(e) shows typical time-resolved spectra obtained in the condition shown in Fig. 4(b)-i in three different time scales to show their details. Four lifetimes were obtained by fitting the signals with exponential functions ($\tau_1 = 24 \pm 5$ ps, $\tau_2 = 203 \pm 34/181 \pm 12$ ps, $\tau_3 = 20 \pm 5$ ns, and $\tau_4 > 500$ ns). The slight differences among the lifetimes obtained in different time scales were within the fitting error. When the polarity of V_{ds} was reversed, as shown in Fig. 4(b)-ii, no signal was observed, which is considered to be due to the flattening the band structure and the charge separation is reduced. These results indicate that the photoinduced signal is generated by not only charge separation but also the change in the band bending, namely photovoltage below the Tip 2 in the WSe_2 region, similar to the detection via SPV in the tip-induced band bending region observed in previous works.[31]

Next, the origin of the lifetimes were considered. Since the charge separation process with the effect of the interface is very fast, <50 fs in the case of WS_2/MoS_2,[32] even if the fast process exists, it is difficult to probe it in this experimental system with the jitter of the two lasers of ~500 fs. However, to analyze the origin of the observed processes, we carried out time-resolved experiment for a pure monolayer WSe_2 sample similarly formed on a SiO_2/Si substrate. Figures 4(c) and 4(f) show the schematic of the experimental setup and obtained result. The lifetimes of the two fast components, τ_1 and τ_2 [picosecond order; Fig. 4(f)] were also obtained when both probes were placed in a WSe_2 region. Namely, these lifetimes may be attributed to the defect-related recombination processes proposed for the case of MoS_2.[29]

On the other hand, when Tip 1 was placed in the $MoSe_2$ region and irradiated with the polarity of V_{ds} reversed, as shown in Fig. 4(d), only the slow components (28 ± 12 ns, 130 ± 19 ns), were observed as shown in Fig. 4(h). The first one (28 ± 12 ns) similar to τ_3 ($=20 \pm 5$ ns, in WSe_2, 16 ± 4 ns in pure WSe_2) is close to the value observed in MoS_2 (10 ns order) which is considered to be the bolometric process.[33] The other components (τ_4: 500 ns < in WSe_2, 130 ± 19 ns in $MoSe_2$) may have been due to the effect of the deep-level trap states considered in the case of $MoSe_2$.[34] It also became difficult to observe the short lifetime components of τ_1 and τ_2 in the WSe_2 region with the aging of the sample. There proposed various mechanisms,[29,33,34] and to understand the mechanism in more detail, it is necessary to investigate, for example, the effects of the excitation wavelength, gate voltage dependence, and sample growth conditions, as related to the local structures. The microscopy method we have developed is useful for carrying out various experiments for such purposes.

In conclusion, by combining scanning MP microscopy with optical methods such as the LMS and OPP methods, we have succeeded in developing a microscopy method useful for measuring electronic structures and photoinduced carrier dynamics in microscopic structures. We demonstrated its performance by analyzing the electronic structures in a monolayer island of a $WSe_2/MoSe_2$ in-plane heterostructure. By observing the FET characteristics and photocurrent mapping over the heterostructure by LMS, we were able to visualize the band structure. The positional dependence of the carrier dynamics was also successfully probed by OPP-MP spectroscopy. Another advantage of this method is that we can observe phenomena with dynamics having wide range of lifetimes from femtosecond to microsecond order or larger. This method is expected to play an important role in the researches to develop advanced functional devices with microscopic structures.

Acknowledgments Supports from Japan Society for the Promotion of Science (Grants-in-Aid for Scientific Research: 17H06088) and CREST are acknowledged.

1) X. L. Qi and S. C. Zhang, Rev. Mod. Phys. **83**, 1057 (2011).
2) K. F. Mak, C. Lee, J. Hone, J. Shan, and T. F. Heinz, Phys. Rev. Lett. **105**, 136805 (2010).
3) W. Choi, N. Choudhary, G. H. Han, J. Park, D. Akinwande, and Y. H. Lee, Mater. Today **20**, 116 (2017).
4) Z. Alpichshev, J. G. Analytis, J. H. Chu, I. R. Fisher, Y. L. Chen, Z. X. Shen, A. Fang, and A. Kapitulnik, Phys. Rev. Lett. **104**, 016401 (2010).
5) S. Yoshida, Y. Kobayashi, R. Sakurada, S. Mori, Y. Miyata, H. Mogi, T. Koyama, O. Takeuchi, and H. Shigekawa, Sci. Rep. **5**, 14808 (2015).
6) H. Mogi, Y. Kobayashi, A. Taninaka, R. Sakurada, T. Takeuchi, S. Yoshida, O. Takeuchi, Y. Miyata, and H. Shigekawa, Jpn. J. Appl. Phys. **56**, 08LB06 (2017).
7) M. Massicotte, P. Schmidt, F. Vialla, K. G. Schädler, A. Reserbat-Plantey, K. Watanabe, T. Taniguchi, K. J. Tielrooij, and F. H. L. Koppens, Nat. Nanotechnol. **11**, 42 (2016).
8) Q. Cui, F. Ceballos, N. Kumar, and H. Zhao, ACS Nano **8**, 2970 (2014).
9) Y. Gong et al., Nano Lett. **15**, 6135 (2015).
10) M. Kolmer, P. Olszowski, R. Zuzak, S. Godlewski, C. Joachim, and M. Szymonski, J. Phys.: Condens. Matter **29**, 444004 (2017).
11) S. Yoshida, Y. Kanitani, O. Takeuchi, and H. Shigekawa, Appl. Phys. Lett. **92**, 102105 (2008).
12) Y. Terada, S. Yoshida, O. Takeuchi, and H. Shigekawa, Nat. Photonics **4**, 869 (2010).
13) H. Mogi, Z. H. Wang, R. Kikuchi, C. H. Yoon, S. Yoshida, O. Takeuchi, and H. Shigekawa, Appl. Phys. Express **12**, 025005 (2018).
14) S. Yoshida, Y. Kanitani, R. Oshima, Y. Okada, O. Takeuchi, and H. Shigekawa, Phys. Rev. Lett. **98**, 026802 (2007).
15) O. Takeuchi, N. Takeuchi, T. Ochiai, H. Kato, S. Yoshida, and H. Shigekawa, Appl. Phys. Express **7**, 021602 (2014).
16) Y. Terada, S. Yoshida, A. Okubo, K. Kanazawa, M. Xu, O. Takeuchi, and H. Shigekawa, Nano Lett. **8**, 3577 (2008).
17) M. Yokota, S. Yoshida, Y. Mera, O. Takeuchi, H. Oigawa, and H. Shigekawa, Nanoscale **5**, 9170 (2013).
18) S. Yoshida, Y. Terada, M. Yokota, O. Takeuchi, H. Oigawa, and H. Shigekawa, Eur. Phys. J. Spec. Top. **222**, 1161 (2013).
19) S. Yoshida, M. Yokota, O. Takeuchi, H. Oigawa, Y. Mera, and H. Shigekawa, Appl. Phys. Express **6**, 032401 (2013).
20) S. Yoshida, Y. Terada, R. Oshima, O. Takeuchi, and H. Shigekawa, Nanoscale **4**, 757 (2012).
21) S. Li, S. Wang, D. M. Tang, W. Zhao, H. Xu, L. Chu, Y. Bando, D. Golberg, and G. Eda, Appl. Mater. Today **1**, 60 (2015).
22) Y. Li, F. Wang, D. Tang, J. Wei, Y. Li, Y. Xing, and K. Zhang, Mater. Lett. **216**, 261 (2018).
23) M. Tosun, S. Chuang, H. Fang, A. B. Sachid, M. Hettick, and Y. Lin, ACS Nano **8**, 4948 (2014).
24) Y. Guo, Y. Ji, H. Dong, L. Wang, and Y. Li, AIP Adv. **9**, 025202 (2019).

25) M. Tosun, L. Chan, M. Amani, T. Roy, G. H. Ahn, P. Taheri, C. Carraro, J. W. Ager, R. Maboudian, and A. Javey, ACS Nano **10**, 6853 (2016).
26) J. Kang, S. Tongay, J. Zhou, J. Li, and J. Wu, Appl. Phys. Lett. **102**, 012111 (2013).
27) Y. Yi, C. Wu, H. Liu, J. Zeng, H. He, and J. Wang, Nanoscale **7**, 15711 (2015).
28) D. Kozawa et al., Nat. Commun. **5**, 4543 (2014).
29) H. Wang, C. Zhang, W. Chan, S. Tiwari, and F. Rana, Nat. Commun. **6**, 8831 (2015).
30) H. L. Liu, C. C. Shen, S. H. Su, C. L. Hsu, M. Y. Li, and L. J. Li, Appl. Phys. Lett. **105**, 201905 (2014).
31) S. Yoshida, Y. Terada, M. Yokota, O. Takeuchi, Y. Mera, and H. Shigekawa, Appl. Phys. Express **6**, 016601 (2013).
32) X. Hong, J. Kim, S.-F. Shi, Y. Zhang, C. Jin, Y. Sun, S. Tongay, J. Wu, Y. Zhang, and F. Wang, Nat. Nanotechnol. **9**, 682 (2014).
33) E. Parzinger, M. Hetzl, U. Wurstbauer, and A. W. Holleitner, npj 2D Mater. Appl. **1**, 40 (2017).
34) K. Chen et al., npj 2D Mater. Appl. **1**, 15 (2017).